SN 2005hj: Evidence for Two Classes of Normal-Bright SNe Ia and Implications for Cosmology[1]

Robert Quimby[2], Peter Höflich[3], J. Craig Wheeler[2]

ABSTRACT

HET Optical spectra covering the evolution from about 6 days before to about 5 weeks after maximum light and the ROTSE-IIIb unfiltered light curve of the "Branch-normal" Type Ia Supernova SN 2005hj are presented. The host galaxy shows H II region lines at redshift of $z = 0.0574$, which puts the peak unfiltered absolute magnitude at a somewhat over-luminous -19.6. The spectra show weak and narrow Si II lines, and for a period of at least 10 days beginning around maximum light these profiles do not change in width or depth and they indicate a constant expansion velocity of $\approx 10,600$ km s^{-1}. Our observations indicate that Si is confined to a relatively narrow velocity region. We analyzed the observations based on detailed radiation dynamical models in the literature. The models considered include delayed detonations, deflagrations, pulsating delayed detonations, and tamped detonation/merger scenarios. Whereas the first two classes of models have been used to explain the majority of SNe Ia, they do not predict a long velocity plateau in the Si II minimum with an unvarying line profile. Pulsating delayed detonations and merger scenarios form shell-like density structures with properties mostly related to the mass of the shell, M_{shell}, and we discuss how these models may explain the observed Si II line evolution; however, these models are based on spherical calculations and other possibilities may exist. SN 2005hj is consistent with respect to the onset, duration, and velocity of the plateau, the peak luminosity and, within the uncertainties, with the intrinsic colors for models with $M_{shell} = 0.2 M_{\odot}$. Our analysis suggests a distinct class of events hidden within the Branch-normal SNe Ia. If the predicted relations between observables are confirmed, they may provide a way to separate these two groups. We discuss the implications of two distinct progenitor classes

[1]Based on observations obtained with the Hobby-Eberly Telescope, which is a joint project of the University of Texas at Austin, the Pennsylvania State University, Stanford University, Ludwig-Maximilians-Universität München, and Georg-August-Universität Göttingen.

[2]Department of Astronomy, University of Texas, Austin, TX 78712, USA

[3]Department of Physics, Florida State University, Tallahassee, FL 32312, USA

on cosmological studies employing SNe Ia, including possible differences in the peak luminosity to light curve width relation.

Subject headings: Supernovae, SN 2005hj, cosmology

1. Introduction

Type Ia supernovae (SNe Ia) are thought to be thermonuclear disruptions of white dwarf (WD) stars (Hoyle & Fowler 1960), but the details remain uncertain. One possibility for the progenitors is the single degenerate model in which main sequence stars or post main sequence red giants transfer mass to a WD through Roche Lobe overflow or a common envelope and the WD grows close to the Chandrasekhar mass M_{Ch}. Due to compression, the thermonuclear runaway starts near the center leading to the explosion of the WD and a rapidly expanding envelope with a mass close to M_{Ch}. A second possibility is the double degenerate model in which a pair of WDs merge and lead to an explosion. In most such cases, the resulting mass of the rapidly expanding envelope will be different from M_{Ch}. Residual material from these mergers surrounding the explosions will get swept up by the ejecta forming dense, shell-like structures. Although the explosion of single WDs seems to be favored for the majority of objects, we may expect mergers to contribute to the SNe Ia population (see §2).

The possibility of different progenitor channels, the population of which may vary with redshift, may pose a challenge for the use of SNe Ia in cosmological studies that rely on a single parameterization, such as a light curve width to peak luminosity relation, LWR, to reduce the intrinsic scatter in the peak magnitudes and render them standard candles (Phillips 1993; Perlmutter et al. 1997). To first order, the LWR relation can be understood as a result of different amounts of ^{56}Ni produced during the explosion (Höflich et al. 1996; Umeda et al. 1999). There may be some spread and an offset in LWR introduced by one of the channels if the masses of the envelope differ from M_{Ch}, and/or the density structures differ. This can lead to a systematic shift of LWR with redshift if the evolutionary time scales of the progenitor systems differ. Even if the different progenitor scenarios obey the same LWR, differences in the color could introduce systematic errors in cosmological studies because SNe Ia are known to suffer to some degree from reddening in their respective host galaxies which has to be taken into account. To correct for this, the maximum light color excess (usually E_{B-V}) and an average reddening law are used to determine the amount of absorption. SNe Ia that are intrinsically redder as compared to the average local sample will thus be over-corrected in this fashion to a higher luminosity.

Similarly to the two distinct progenitor channels, qualitative variations in the explosion physics may lead to various classes of SNe Ia even within the single degenerate scenarios. Standard explosion models include delayed detonations (DD) and deflagrations. In these scenarios, burning during the deflagration phase leads to an unbound WD. In DD models, the deflagration turns into a detonation in an expanding envelope. Because the density structure of the WD declines monotonically with radius, the resulting density structure in the expanding envelope also smoothly declines with mass and radius. A variation of DD models are the pulsating delayed detonation models (PDD; Khokhlov et al. 1993; Höflich et al. 1995a). In these models, the total energy production during the deflagration phase is, by construction, lower and insufficient to unbind the WD. This results in large amplitude pulsations. Because the fall-back time increases with distance, the inner regions contract and leave a shell behind at larger distances. Due to infall driven compression, a detonation is triggered, the material behind the burning front is accelerated, and this expanding material runs into the low-velocity material left at larger distances. Similar to the merger scenario, a shell-like structure is formed with very similar light curve and spectroscopic properties, but with a total mass close to M_{Ch} (Höflich & Khokhlov 1996).

These two groups, consisting of DD and deflagration models such as W7 (Nomoto et al. 1984), which lack shells, and the models with shells (mergers and PDDs), can be differentiated by their predictions for the photospheric evolution and maximum light colors (Khokhlov et al. 1993; Höflich & Khokhlov 1996). For the former group, the photospheric velocities, v_{ph}, smoothly decline with time and the models show a blue color at maximum light, $B-V \approx 0^m$; in the latter group, v_{ph} shows a plateau in the evolution as the photosphere recedes through the shell. These models are intrinsically redder and slightly over-luminous because of the lower expansion rate in the inner region. As shown in Khokhlov et al. (1993) the color, length and velocity of the plateau are correlated with the mass of the shell, and this potentially allows the two groups to be distinguished even for similar brightnesses.

Indeed, there is a growing sample of SNe Ia showing photospheric velocity plateaus (e.g. 1990N; Leibundgut et al. 1991; Mueller & Höflich 1994; 1991T, 1999aa; Garavini et al. 2004; 1999ee; Hamuy et al. 2002; 2000cx; Li et al. 2001a; see also Benetti et al. 2005). Many of these SNe Ia have been reported as having a red color $B-V$ at maximum, but this is typically attributed to reddening along the line of sight. Alternatively, this sample may suggest the contribution of events with shell-like density structures in the observed population. These events may be understood in terms of mergers or PDDs; however, the inhomogeneities and incompleteness of individual data sets in the literature preclude definite conclusions.

To address this problem and others, we started the Texas Supernovae Search (TSS; Quimby et al. in prep.) with the goal of providing a homogeneous set of quality data for

several supernovae beginning well before maximum light. In this paper, we present our observations of SN 2005hj and analysis of the data. In §2 we describe the discovery and give the details for both the photometric and spectroscopic follow-up. In §3 we discuss generic properties of explosion models and suggest a secondary parameter to separate models with and without shells, and analyze the peculiarities of SN 2005hj. Conclusions and discussion are presented in §4.

2. Observations

SN 2005hj was discovered on October 26.13 UT in the field of Abell 194 as part of the TSS. The TSS uses the wide field ($1\overset{\circ}{.}85 \times 1\overset{\circ}{.}85$) 0.45m ROTSE-IIIb telescope (Akerlof et al. 2003) at the McDonald Observatory in Texas to scan nearby galaxy clusters nightly for transients with a modified version of the PSF-matched image subtraction code from the Supernova Cosmology Project. SN 2005hj was found at an unfiltered magnitude (calibrated against the USNO-B1.0 R2) of $C_R = 17.4$ and is located at $\alpha = 01^h26^m48\overset{s}{.}27$, $\delta = -01^\circ14'16\overset{''}{.}8$. The foreground reddening at this location is $E_{B-V} = 0.039^m$ (Schlegel et al. 1998). Examination of ROTSE-IIIb images from Oct. 20 and Oct. 22 shows the SN was detected prior to discovery, but not significantly well to pass the search pipeline's automatic cuts. Figure 1 shows the ROTSE-IIIb light curve for SN 2005hj through 40 days after maximum light. To construct the light curve, we co-added images taken on a given night (usually 6) excluding any frames of significantly lower quality due to passing clouds or wind sheer, and then subtracted the reference image convolved to the same PSF. Magnitudes were determined by fitting the local PSF (derived from the co-added nightly images) to the location of the SN on the subtracted frame using custom software and the DAOPHOT PSF-fitting routines (Stetson 1987 ported to IDL by Landsman 1989).

The unfiltered CCD response of ROTSE-IIIb has an approximate full width of ~ 4000 Å centered in the R-band around 6000 Å. Because we do have some sensitivity in the blue and since the $B - V$ colors of SNe Ia typically grow ~ 1.0 mag redder in the 30 days after maximum (Phillips et al. 1999; Krisciunas et al. 2003), there is a blue deficit at later times that causes our unfiltered magnitudes to decline more rapidly than the true R-band fading. Note that $V - R$ colors of SNe Ia are close to zero at maximum light. We therefore limit the light curve fitting to data taken before 10 days after maximum (determined through several iterations of the fit), during which the color evolution is minimal. The best fit R-band template from Knop et al. (2003) is also shown in Figure 1. The date of maximum light determined from the fit is Nov. 1.6 with a formal error of 0.7 days (note the template phases are relative to the B-band maximum). The best fit stretch factor (Perlmutter et al. 1997) for

the light curve width is $s = 1.2 \pm 0.1$. The preliminary measurement of the observed $B - V$ color at V maximum from the Carnegie Supernova Project is $0.07^m \pm 0.05$ after removal of the host light but before any extinction or k-corrections are applied (M. M. Phillips, private communication).

Near real-time photometric analysis combined with target of opportunity (ToO) time on the neighboring 9.2m Hobby-Eberly Telescope (HET) allowed us to obtain optical spectra just 4 hours after the discovery images were taken and every few days over the next 6 weeks. These observations are detailed in Table 3. The instrumental response is such that very little second order light is expected blue of 8900 Å even with the GG385 blocking filter. The data were reduced in the optimal manner using IRAF[1] and custom IDL scripts. The wavelength scale was calibrated against Cd and Ne lamps and its accuracy was verified by comparing night sky lines to the spectral atlas of Hanuschik (2003). Because the HET pupil size varies for different tracks, absolute flux calibration cannot reliably be achieved; however, we used the standard stars of Massey et al. (1988) and Massey & Gronwall (1990), which were observed using the same setups, to achieve *relative* spectrophotometric calibration and to remove strong telluric features.

The redshift of the host galaxy was derived from narrow emission lines around 7000 Å (observed), which we attribute to H-α, [N II], and [S II] in the host galaxy. We combined all the spectra and simultaneously fit these lines with Gaussians to determine the line centers. The line redshifts are best fit by $z = 0.0574 \pm 0.0002$, and we adopt this value for the SN. This gives SN 2005hj an absolute peak magnitude of -19.6 in our unfiltered band pass (assuming H_0=71 km s^{-1} Mpc^{-1}, $\Omega_m = 0.3$, and $\Omega_\Lambda = 0.7$), and places the host well behind Abell 194 ($z = 0.0180$; Struble & Rood 1999). The brightness and broad light curve shape suggest that SN 2005hj is a slightly over-luminous SN Ia.

The unfiltered ROTSE-IIIb reference image shows that the host for SN 2005hj is relatively bright ($C_R = 17.8$) and compact, and is therefore likely a significant contaminant to our spectra. Thus, we have to subtract the galaxy contribution (see Fig. 2). Lacking an observed spectrum for the host galaxy excluding the SN light, we constrained the galaxy SED using archival Sloan Digital Sky Survey (SDSS) *ugriz* observations and obtained a template galaxy spectrum (N. Drory 2005, private communication). The relative amounts of SN and galaxy light in the spectral apertures will vary not only with the changing SN brightness, but also with the seeing, slit width and positioning. Also plotted in figure 2

[1]IRAF is distributed by the National Optical Astronomy Observatories, which are operated by the Association of Universities for Research in Astronomy, Inc., under cooperative agreement with the National Science Foundation.

is a spectrum of SN 1999aa (blue curve) constructed via a linear interpolation of the −7 day and −3 day spectra presented by Garavini et al. (2004). Noting the similarity of the spectral features of SN 1999aa and SN 2005hj, we assume that we can model our observed spectra as a linear combination of our galaxy template and the SN 1999aa spectra interpolated to the same phase as the SN 2005hj observations. We perform a least squares fit to determine the relative contributions of each component. The red line in figure 2 shows the derived contribution of galaxy light in the −6 day spectrum. Aside from a few small differences (most noticeably in the Mg II λ4481 triplet), some of which may be explained by calibration errors, the combined SN 1999aa + host spectrum (purple curve) is a good fit. The over all fit is improved if we interpolate the SN 1999aa spectra to −5 days instead of −6, especially in the 5400 Å to 6500 Å range, which could imply a ∼1 day error in the date of maximum light or different time scales for the spectral evolutions of the two SNe. We repeated this process for all the SN 2005hj spectra, each time using the same galaxy template and the SN1999aa spectra (interpolated to the appropriate phase) as reference to determine the relative amount of galaxy light. In general, the galaxy template added to the SN 1999aa spectra does an excellent job of reproducing the observed SN 2005hj spectra. The galaxy light typically dominates the flux red of 7000 Å. Figure 3 shows the spectral evolution of SN 2005hj recorded by the HET between days −6 and +34 with the derived galaxy contribution subtracted.

2.1. Spectral Characteristics of SN 2005hj

Overall, SN 2005hj shows spectra with lines dominated by intermediate mass and iron group elements as is typical for SNe Ia. While the lines show normal expansion velocities, the absorption components are more narrow and, for the early phases, weaker than typically observed, as exemplified by the Si II λ6355 line (see Fig. 4). SN 2005hj also shows an atypical velocity evolution of these features over time.

Line minima are useful diagnostic indicators of the ejecta structure as they give the abundances and velocities of the material. The actual measurement of the velocity at the minimum of the line profile is complicated by the presence of the continuum, other blended lines, and some uncertainty in the true line profile shape. Detailed modeling is required to accurately sort out all the components and how they relate to the photospheric layer to reveal the velocity distribution of the ejecta[2]. Such models have shown that the absorption minima

[2]In general, Si II lines form above the photosphere and velocities measured from such absorption minima can be 1000 to 2000 km s^{-1} larger than those measured from weak lines. However, for shell models the steep

approximate the photospheric expansion velocities to within about 1000 km s^{-1} at maximum light (Höflich et al. 1995a; Marion et al. 2006). Thus, simple line fitting can lead to a rough description of the ejecta velocities, and allows a useful comparison to discriminate between different models. At late times the photosphere will recede below the Si rich layer and so the velocities derived from the Si II λ6355 line will become increasingly discrepant with the photospheric velocity. For deflagration and classical detonation models, this departure will begin to set in 1-2 weeks after maximum light (Höflich & Khokhlov 1996).

The strength of the Si II λ6355 line and its persistence from at least 2 weeks before to 4 weeks after maximum light make it a valuable tool for probing the ejecta. Its evolution with time is shown in figure 5 for the case of SN 2005hj. To determine the velocity, we smooth the spectra by Fourier Transform filtering, divide by the estimated continuum, and then select the lowest point using spline interpolation over a selected range. The continuum is represented by a medium order (6th - 7th) polynomial fit to regions of the spectra that are not strongly affected by lines. To smooth the spectra, we use a Fourier Transform to convert the data into a power spectrum, and then multiply this by a filter to remove high frequency variations. We then apply a reverse FT to the filtered power spectrum to recover the smoothed spectrum. The filter has the functional form

$$\Phi(\nu) = \begin{cases} 1 & \text{for } -\nu_{\rm c} \leq \nu \leq \nu_{\rm c} \\ \exp[-(\nu-\nu_c)^2/2\sigma^2] & \text{otherwise} \end{cases} \quad (1)$$

The filter cutoff frequency, ν_c, and attenuation scale, σ, were determined as follows: 1) the spectra were converted into a power spectrum, $P(\nu)$, via Fourier Transform; 2) the slope of $\log(P)$ is fit over the noise dominated high frequencies and interpolated through the low frequencies to determine the noise spectrum; 3) ν_c is taken as the frequency at which $\log(P)$ drops to within three times the dispersion about the noise spectrum; 4) σ is chosen such that the slope of $\log[P(\nu_c + 2\sigma)]$ is twice the noise spectrum slope (i.e.. $\nu = \nu_c + 2\sigma$ is the frequency above which noise is clearly the dominate component). For this analysis, only the spectral bins with signal to noise above 25 were considered (note the peak throughput for HET/LRS is near the Si II λ6355 line). For consistency, we adopt a single filter for all our analysis, choosing the results from our nosiest data, $\nu_c = 0.0066$ Å^{-1} and $\sigma = 0.0053$ Å^{-1}, which removes noise in the data but also some real information related to "sharp" features in the spectra such as the narrow core to the Si II λ6355 absorption in the day +10 spectrum.

Using the relativistic Doppler formula and the gf-weighted Si II λ6355 rest velocity in the host galaxy frame, we convert the wavelengths of the line profile minima into expansion

---

density gradients cause even strong lines to from very close (in radius) to the actual photosphere.

velocities. For each spectrum we conducted 250,000 Monte Carlo simulations in which normally distributed noise based on the statistical flux errors was added to the data and the FT smoothed minimum was found. The peak of the distribution and the interval containing 68% of the simulation results were used to calculate the velocity of the minimum and its error, respectively. We also measured the relative shift in the H II region lines over all epochs and found the scatter to be 80 km s^{-1}, which we add in quadrature to the individual errors. The results are given in table 2 and plotted in figure 6. We find that the data points are at 10,600 $\pm$ 150 km s^{-1} between maximum light and +18 days, somewhat faster prior to maximum, and significantly slower on day +25. By day +34, the Si II λ6355 absorption has all but completely disappeared.

From maximum light through day +10, the Si II λ6355 line profile shows little change in both depth and width in addition to maintaining a constant absorption minimum velocity. Of specific relevance is the blue wing of the absorption profile; this section of the line is formed by the material at the greatest distance from the photosphere and at the highest velocities, and as such it should be the first to vanish as the photosphere recedes. The consistency of this blue wing from maximum light through day +10 suggests the photosphere falls within the Si enriched layers for at least this period. By day +18 the blue wing has shifted significantly to the red, while the red wing remains constant except for the effects of an Fe II blend around 6250 Å. Other Fe II features begin to appear or strengthen at this phase as well. This behavior could be a signal that the Si layers are becoming detached from the photosphere by day +18.

The day +25 spectra show a double minimum at the location of the Si II λ6355 feature (see figure 7). Telluric absorption is weak in this wavelength range, and the line profile is clearly seen in each of the three individual exposures, which support the reality of this feature. A possible explanation for this feature is contamination from the host that is not removed by the template subtraction; however, galaxy spectra do not typically exhibit features in this range that could cause such interference, and even if such were the case, we would expect to see similar behavior in the +34 day spectra. A second possibility is contamination from Fe II lines. Using the spectral analysis tool SYNOW (Jeffery & Branch 1990; Fisher et al. 1997, 1999), and the example of SN 1994D as a starting place (Branch et al. 2005), we find that while Fe II likely produces the absorption dips $\sim$ 100 Å away on either side of the Si II λ6355 line, it is unlikely responsible for the double minimum. The third possibility, which we favor, is that this double minimum simply appears because we are resolving the Si II λ6355 doublet. This result implies that the Si II seen in the +25 day spectra is confined to a very narrow region of velocity space ($\Delta v \approx 1,500$ km s^{-1}). If accurate, the true minimum of the Si II λ6355 doublet would be about 100-200 km s^{-1} faster than indicated in figure 6 and table 2, but still significantly below the plateau velocity. The emergence of this thin layer may

also be responsible for the appearance of the narrow core in the +10 day spectrum as well as the apparent double minimum to the +18 day data. Some remnant of the blue component to the doublet may persist to the +34 day spectrum. Figure 7 also shows the spectra of several other SNe Ia taken around 25 days after maximum light. While the distinctly double minimum appears unique to SN 2005hj, the width and depth of the Si II feature is roughly consistent with the others.

SN 2005hj clearly belongs to the low velocity gradient (LVG) group in the classification scheme of Benetti et al. (2005), but moreover the velocity derivative from maximum light through day +18, $\dot{v} = 3 \pm 7$ km s^{-1} day^{-1}, is consistent with no change[3]. From the line profile evolution (table 2, figures 5 and 6) we can deduce a plateau phase starting at -2.5 ± 2.5 days which lasts no more than 30 days. Noting the change in the Si II λ6355 line profile in the +18 day spectrum, we conservatively mark the end of the plateau phase as day 17.5 ± 7.5 days, which gives the plateau phase a total duration of 20 ± 10 days. The Si II λ6355 velocity evolution derived from the minima of FT smoothed spectra of several selected SNe Ia is plotted in figure 8. The velocity plateau of SN 2005hj is similar to that of other over-luminous SNe Ia such as SN 1999aa (Garavini et al. 2004) and SN 2000cx (Li et al. 2001a), but it is distinct from normal SNe Ia such as SN 1994D (Patat et al. 1996) and SN 1992A (Kirshner et al. 1993) that do not show a plateau phase[4].

3. Physical Constraints from Explosion Models

There is general agreement that SNe Ia result from some process involving the combustion of a degenerate C/O white dwarf (Hoyle & Fowler 1960). Within this general picture, two classes of models are most likely. The first is an explosion of a C/O-WD with a mass close to the Chandrasekhar limit (M_{Ch}) that accretes matter through Roche-lobe overflow from an evolved companion star (Whelan & Iben 1973). In this case, the explosion is triggered by compressional heating near the WD center. Alternatively, the SN could be an explosion of a rotating configuration formed from the merging of two low-mass WDs, after the loss of angular momentum (Iben & Tutukov 1984; Paczynski 1985). Candidate progenitor systems have been observed for both scenarios: WD binary systems with the correct period to merge

[3]As defined by Benetti et al. (2005), $\dot{v}$ is the average daily rate of decrease in the expansion velocity from maximum light through the last available spectrum before the Si II λ6355 line disappears; therefore, including the day +25 spectrum, SN 2005hj formally has $\dot{v} = 27 \pm 4$ km s^{-1} day^{-1}, but with a χ^2 per degree of freedom of 3.2

[4]We removed the data point at day −3 from the SN 1999aa curve because all spectral features in these data seem to be frequency shifted including the telluric features.

in an appropriate time scale with an appropriate total mass (Maxted et al. 2000); and supersoft X-ray sources (Greiner et al. 1991; van den Heuvel et al. 1992; Rappaport et al. 1994; Kahabka & van den Heuvel 1997) showing accretion onto the WD from an evolved companion. There are still open questions about the details of both the merging and accretion processes (e.g. Nomoto 1982; Benz et al. 1990; Piersanti et al. 2003; Nomoto et al. 2003).

From the observed spectral and light curve properties, the first scenario appears to be the most likely candidate for the majority of normal SNe Ia. In particular, delayed detonation (DD) models (Khokhlov 1991; Yamaoka et al. 1992; Woosley & Weaver 1994) have been found to reproduce the majority of the observed optical/infrared light curves (LC) and spectra of SNe Ia reasonably well (Höflich 1995; Fisher et al. 1995; Höflich & Khokhlov 1996; Lentz et al. 2001; Höflich et al. 2002; Marion et al. 2003, 2006). In the DD scenario, a slow deflagration front turns into a detonation. The WD pre-expands during the deflagration and undergoes complete burning during the detonation phase. Similarly, the classical deflagration models W7 (Nomoto et al. 1984) show similar behavior to DDs but only by neglecting instabilities due to the deflagration fronts (Gamezo et al. 2003). For recent reviews see Branch (1998); Hillebrandt & Niemeyer (2000); Höflich (2006).

Despite the success of classical DD and W7 models, both lack the basic features seen in SN 2005hj. Neither predicts a long plateau in velocity; they instead show a smooth decline of the photospheric velocity[5] as a function of time (Fig. 9). This happens because in expanding envelopes the photosphere recedes in mass and, because of the homologous expansion, in velocity as well. This behavior results from the smoothly declining density structure of the WD and the fact that variations in the specific energy production are small.

In contrast, shell-like density structures will produce velocity plateaus in a natural way because the photosphere remains in the shell for some time as shown by Khokhlov et al. (1993); Höflich & Khokhlov (1996). To form a shell-like structure requires interaction of rapidly expanding material with a surrounding envelope. Various mechanisms have been suggested to supply this surrounding matter: the pulsating delayed detonation scenario (Höflich et al. 1996), mergers or tamped detonation models. Shells may also form by the interaction of an exploding single WD within the progenitor system (Gerardy et al. 2004; Quimby et al. 2006).

[5]Although the Si II λ6355 line is an imperfect tracer of the photospheric velocity as mentioned in §2.1, the observed SNe Ia population typically exhibits a 1000-3000 km s^{-1} decrease in the measured line velocities between 1 week before maximum light to 2 weeks after(Branch et al. 1988; Benetti et al. 2005), and the deflagration and classical delayed detonation models employed to explain these events have shown a correspondingly large decrease in photospheric velocities over the same period (Khokhlov et al. 1993). These models are inconsistent with the corresponding $\approx$ 300 km s^{-1} shift measured for SN 2005hj.

We analyzed the observations of SN 2005hj based on detailed, spherical models for supernovae published in the literature. The models are based on detailed calculations for the explosion, light curve and spectra. The models considered include delayed detonations, deflagrations, pulsating delayed detonations and tamped detonation/merger scenarios. In figure 9, we show the photospheric velocities as a function of time for these models along with the Branch-normal SNe Ia to illustrate the formation of a plateau in the models that naturally form a shell. Note for lower shell masses, this "plateau" is more accurately described as a period of slowly declining velocities.

In classical delayed detonation models and for normal-bright SNe Ia, Si is present over a wide range in mass, spanning about 0.4 to $0.5 M_{\odot}$, which corresponds to velocities from about 8,000 to 9,000 km s^{-1} to more than 20,000 km s^{-1}. The Si layer is thick (in the mass frame) because explosive oxygen burning occurs over a wide range of temperatures. The density gradient is smooth and Si is mostly in Si II, so initially the velocity derived from the minimum of the Si II λ6355 line smoothly declines with the receding photosphere governed by the geometrical dilution of the expanding envelope. Eventually, the photosphere begins to recede below the Si layer at which point the evolution of the Si II λ6355 line profile will show the following behavior: 1) the optical depth of the highest velocity material at the largest radii will begin to decline below 1 and as such the blue wing of the line profile will start to drift toward the red; 2) as the optical depth decreases, the strength of the line as measured from the line depth will decrease; 3) the line minimum may continue to slow, but it will grow increasingly discrepant with the photospheric velocity. This phase typically begins 1-2 weeks after maximum light for normal SNe Ia and is heralded by the appearance of Fe II lines. While this behavior is commensurate with observations of normal-bright SNe Ia such as SN 1994D, this behavior is not consistent with the observations of SN 2005hj.

The Si II λ6355 line seen in SN 2005hj is narrow, and during the plateau phase the wings do not change, the depth does not change, and the velocity of the minimum does not change to within the errors. The data require a narrow distribution of Si II in velocity space, and we suggest this may be explained by an interaction that compresses the Si rich layers as predicted by merger and pulsating delayed detonation models. The shell models are also consistent with the velocity drop seen after the plateau because a significant amount of Si is located below the shell (Khokhlov et al. 1993; Höflich & Khokhlov 1996).

In Fig. 10, we show general properties of these models. As discussed in the papers above, to first order, the observational signatures of the shell depend on the mass of the shell M_{shell}. Almost the entire WD is burned, and momentum conservation determines the amount of high velocity matter that can pile up in the expanding shell. With increasing shell mass, more material of the SN envelope is slowed down. As a consequence, the velocity of

the shell v_{shell} decreases with M_{shell}. Because it will take longer for the photosphere to recede into the lower velocity matter, the time until the beginning of the plateau phase, t_0, increases with M_{shell}. The optical depth increases with M_{shell}, duration of the plateau, Δt_{shell}, also increases, the temperature gradient becomes steeper, and the photosphere becomes cooler (i.e. $B-V$ increases) with increasing M_{shell} (Khokhlov et al. 1993; Höflich & Khokhlov 1996). The duration of the plateau, Δt_{shell}, is defined by the velocity spread δv around v_{Shell} with $\delta v = 500$ km s^{-1}, which puts the end of the plateau phase safely into the parts of a rapidly declining v_{ph}. We choose a larger value than in the observations to avoid ambivalences due to discreetness, which, in some of the models, is of the order of ≈ 100 km s^{-1}. By increasing δv from 200 to 500 km s^{-1} the nominal duration is increased by ≈ 1 day. However, we also note that the actual width depends on the velocity spread in the shell (see §4).

Given the model predictions, we can use different observational indicators to test which M_{shell} is consistent with SN 2005hj (Fig. 10). All three parameters, v_{shell}, t_{shell}, and t_0 suggest $M_{shell} \approx 0.2 M_\odot$, with the allowed ranges specifically bracketed by 0.15-0.6, 0.1-0.25, and 0.1-0.25 $M_\odot$ for the plateau length, shell velocity, and plateau onset, respectively, taking the observed errors into account. The comparison between the $B-V$ color as a function of v_{shell}, t_{shell}, or t_0, however, shows only marginal consistency between the observations and the models if we assume only foreground redding by the Galaxy. We note, that the intrinsic $B-V$ color of the models is uncertain by about 0.05 to 0.1^m at maximum light. The two best-fitting models, `pdd3` and `det2env2`, show a peak brightness, M_V, of -19.42^m and -19.41^m, respectively, with an uncertainty of $\approx 0.1^m$ (Höflich & Khokhlov 1996) vs. a typical DD model with -19.2^m (Höflich et al. 2002), i.e. they are brighter by about 20 % mostly due lower escape probablity of γ-rays that results when the ^{56}Ni layers are slowed down because of the interaction (Höflich et al. 1991).

4. Discussion and Conclusions

We have presented photometric and spectroscopic data for SN 2005hj, a slightly over-luminous Type Ia. The most striking feature is an apparent plateau in the expansion velocity evolution, which we derive from the Si II λ6355 line. The velocities remain at about $10,600$ km s^{-1} for about 3 weeks starting slightly before maximum light, and this plateau is bracketed by preceding and succeeding decelerations. We find that Si is confined to a relatively narrow velocity region. Analysis of the detailed observations in concert with published models suggest there may be some physical distinction between SN 2005hj and other normal-bright SNe Ia that may systematically affect their use as distance indicators if not properly taken

into account.

The models considered include delayed detonations, deflagrations, pulsating delayed detonations and tamped detonation/merger scenarios. In order to explain the narrow Si II λ6355 line and its plateau in velocity, we suggest an early interaction that forms a dense shell as predicted by merger and PDD models. The spectral and photometric peculiarities are consistent with respect to the velocity, duration, and onset of the plateau, and marginally consistent with the maximum light color, for models that have shells of about $0.2 M_{\odot}$. As indicated by earlier works (Khokhlov et al. 1993; Höflich & Khokhlov 1996), the mass of the interacting shell has been found to be the parameter that dominates the details of these observational signatures independent of how this shell may form. The tight predicted relation between each of v_{shell}, t_{shell}, and t_0 may provide a stable means to separate SN 2005hj like events from regular Branch-normal SNe Ia. Although the agreement between the shell models and the observations is good, the predictions are not necessarily unique and other possibilities may exist. For example, we have not considered 3-D models such as the detonation from a failed deflagration scenario recently examined by Kasen & Plewa (2006). For SN 2005hj then the agreement of the plateau velocity and its duration to that predicted by shell models may simply be a fluke, and in such case this concordance should then not hold for other SNe with similar Si II λ6355 evolution. Given the data and models considered, we suggest either PDDs or merger events are responsible for SN 2005hj, and this implies the existence of two different progenitor channels.

It is important to understand how these two progenitor channels, which may occur in relatively varying fractions as a function of redshift, will impact studies using SNe Ia as distance indicators. Li et al. (2001b) estimate that 20% of SNe Ia in their sample are either 1991T-like or 1999aa-like. These SNe show spectral features and a velocity plateau similar to SN 2005hj. Branch (2001) found 5 1999aa-like events in the Li et al. (2001b) sample out of 20 total SNe Ia that were observed early enough to show 1999aa-like spectral features, and one that was 1991T-like; however, in the pre-LOSS sample they do not classify any of the 7 SNe Ia with early spectra as 1999aa-like. These nearby samples are constructed from targeted galaxy searches that have different selection biases than the deep cosmological surveys, but we will assume a uniform 2005hj-like rate of 25% for all SNe Ia. SNe Ia that appear spectroscopically similar to SN 2005hj in a single epoch could none the less arise from different progenitors, and the mass of the low-density envelope around PDDs or mergers may effect their peak magnitudes and/or light curve shapes, but we will further assume that all such events deviate uniformly from the LWR of Branch normal SNe Ia. Höflich et al. (1996) calculated the relation between peak V band magnitudes, M_V, and the fading between maximum light and +20 days, $dM_V(20)$, for a variety of theoretical models and found that shell models produced $dM_V(20)$ that were 0.2 to 0.3 mag smaller than for (in vacuum)

delayed detonations reaching the same peak magnitude. Therefore using the same LWR for shell models will result in corrected peak magnitudes systematically offset by 0.1 to 0.2 mag. Also, the observed peak magnitudes of SNe Ia are usually corrected for absorption along the line of sight using the observed $B-V$ color at maximum light and a reddening law. For events that are intrinsically red, this will increase the estimated peak magnitude above its already over-luminous intrinsic value. Cosmological studies may therefore need to remove or at least separately handle SN 2005hj-like events to avoid systematic errors in distance.

As a case for the importance of separating different progenitors, let us consider SN 1999ee. Very similar to SN 2005hj, SN 1999ee shows a plateau with $v_{shell} = 10,500$ km sec^{-1}, a duration of 14 ± 3 days, and an onset at day -3 ± 1 relative to maximum (Hamuy et al. 2002; see Fig. 8). The $B-V$ color of SN 1999ee was also quite red at maximum light; $+0.28^m \pm 0.04$ after correction for galactic extinction (Stritzinger et al. 2002; Krisciunas et al. 2004). Based on the standard brightness decline relation and the corresponding colors, Hamuy et al. (2002) derived reddening in the host galaxy of 0.28 ± 0.04 which implies an absolute brightness of $M_V = -19.95^m$ similar to SNLS-03D3bb which Howell et al. (2006) attributed to a super-Chandrasekhar mass WD. Taking into account the spectroscopic information about the velocity plateau, its length and onset, we attribute a portion of the red color to the intrinsic properties of the supernova. We find that the duration of the velocity plateau, its onset and size are consistent with a shell mass of $0.2 M_\odot$ which suggests an intrinsic color $B-V$ of $0.15^m \pm 0.02$ (see Fig. 10). This reduces the reddening in the host galaxy to $\approx 0.13^m$ and the absolute brightness M_V to -19.53^m, which compares favorably to the model predictions of -19.42^m and -19.41^m for `pdd3` and `detenv2`, respectively, within the model uncertainties. Note that there is an interstellar sodium line in the spectra that implies some degree of reddening within the host. There are some apparent spectral differences when compared to SN 2005hj, namely SN 1999ee has a slightly broader blue wing in Si II and stronger absorption around 4900 Å. This may either hint toward different explosions scenarios (i.e. pulsations versus mergers), or different viewing angles of asymmetric envelopes.

This brings us to the limitation of our studies. Except for the color, SN 2005hj fits remarkably well with the merger and PDD model predictions but, still, it is a single event and the good agreement may be coincidental. We need a large, well-observed sample of similar objects to test and verify or falsify the models and to determine the shell mass distribution. Moreover, 3D effects have been neglected. In reality, we must expect some dispersion. Though pulsating delayed detonation models may be expected to be rather spherical, mergers may be asymmetric with directionally dependent luminosities and colors. In fact, both classes may be realized in nature. As mentioned above, the duration of the plateau, Δt_{shell}, is defined by the velocity spread around v_{Shell}. The physical width of the shell depends, to first order, on the distance at which the interaction occurs and the density

distribution of the interacting expanding media and shell during the hydrodynamical phase of the interaction (Gerardy et al. 2004). For obvious reasons, asymmetries of the shell will increase the velocity gradient seen over the shell. The observations of SN 2005hj indicate a very flat plateau that, in principle, may further constrain the properties of the shell. For SN 2005hj, this may already indicate a rather spherical shell and hint toward the PDD scenario or mergers with an intermediate disk of very large scale heights. However, additional information needs to be taken into account such as detailed line profiles and statistical properties to break this degeneracy between mergers and PDDs.

As a next step, detailed models for the explosion, light curves and spectra tailored toward individual events need to be constructed. Whereas the mean velocity of the shell for a given mass is dictated by momentum conservation, the thickness of the shell is limited by the distance of the shell material, the distance sound can travel during the interaction, and the specific density profile within the shell. With increasing distance of the shell, the relative size (and corresponding velocity spread) becomes smaller because the sound speed remains about the same. The intrinsic color will be sensitive to the optical depth of the shell, which is governed by the magnitude of the density jump and thus depends on the distance of the interacting shell from the WD (Gerardy et al. 2004). The blue $B - V$ color for SN 2005hj may hint of a need to modify the distance and structure of the shell. Precise analysis of such "non-stable" features requires detailed model fitting beyond the scope of this paper.

In the recent past, both the scenarios leading to shell-like structures have been discounted. PDD models have been dismissed because 3D deflagration models showed that the WD becomes unbound and thus pulsations would not occur (Röpke et al. 2003; Hillebrandt & Niemeyer 2000). However, it has recently been shown that this solution depends mainly on the ignition conditions, namely the number and locations of ignition points leading to single or multiple bubble solutions, and mixture of bubble solutions leading to Raleigh-Taylor instabilities. As a result, solutions with fewer bubbles are likely to result in a reduced amount of burning, thus only slightly unbinding the WD and increasing the possibility of PDDs (Livne et al. 2005; Plewa et al. 2004). Similarly, the merging scenario has been dismissed because the WD may undergo burning during the merger and result in an accretion induced collapse (Nomoto & Kondo 1991), and also on the basis of the long merging time scale. However both of these results depend sensitively on the initial conditions, and new pathways to the actual merging may effect the results (Lü et al. 2006). In light of our results, the predicted death of both of these scenarios may be premature, and further studies are needed.

We would like to thank the staff of the Hobby-Eberly Telescope and McDonald Observatory for their support and the ROTSE collaboration. We give specific thanks to J. Caldwell, S. Odewahn, V. Riley, B. Roman, S. Rostopchin, M. Shetrone, E. Terrazas, and M. Villarreal

for their skilled observations with the HET, and to F. Castro, P. Mondol, and M. Sellers for their efforts in screening potential SN candidates. This work made use of the SUSPECT online database of SNe spectra (`http://bruford.nhn.ou.edu/$\sim$suspect/index1.html`). This research is supported, in part, by NASA grant NAG 5-7937 (PH) and NSF grants AST0307312 (PH) and AST0406740 (RQ & JCW).

REFERENCES

Akerlof, C. W., Kehoe, R. L., McKay, T. A., et al. 2003, PASP, 115, 132

Benetti, S., Cappellaro, E., Mazzali, P. A., et al. 2005, ApJ, 623, 1011

Benz, W., Cameron, A. G. W., Press, W. H., & Bowers, R. L. 1990, ApJ, 348, 647

Branch, D. 1998, ARA&A, 36, 17

—. 2001, PASP, 113, 169

Branch, D., Baron, E., Hall, N., Melakayil, M., & Parrent, J. 2005, PASP, 117, 545

Branch, D., Drucker, W., & Jeffery, D. J. 1988, ApJ, 330, L117+

Elias-Rosa, N., Benetti, S., Cappellaro, E., et al. 2006, MNRAS, 369, 1880

Fisher, A., Branch, D., Hatano, K., & Baron, E. 1999, MNRAS, 304, 67

Fisher, A., Branch, D., Höflich, P., & Khokhlov, A. 1995, ApJ, 447, L73+

Fisher, A., Branch, D., Nugent, P., & Baron, E. 1997, ApJ, 481, L89+

Gamezo, V. N., Khokhlov, A. M., Oran, E. S., Chtchelkanova, A. Y., & Rosenberg, R. O. 2003, Science, 299, 77

Garavini, G., Folatelli, G., Goobar, A., et al. 2004, AJ, 128, 387

Gerardy, C. L., Höflich, P., Fesen, R. A., et al. 2004, ApJ, 607, 391

Greiner, J., Hasinger, G., & Kahabka, P. 1991, A&A, 246, L17

Hamuy, M., Maza, J., Pinto, P. A., et al. 2002, AJ, 124, 417

Hanuschik, R. W. 2003, A&A, 407, 1157

Hillebrandt, W. & Niemeyer, J. C. 2000, ARA&A, 38, 191

Höflich, P. 1995, ApJ, 443, 89

Höflich, P. 2006, Nuclear Physics A, 777, 579

Höflich, P., Gerardy, C. L., Fesen, R. A., & Sakai, S. 2002, ApJ, 568, 791

Höflich, P. & Khokhlov, A. 1996, ApJ, 457, 500

Höflich, P., Khokhlov, A., Wheeler, J. C., et al. 1996, ApJ, 472, L81+

Höflich, P., Khokhlov, A. M., & Wheeler, J. C. 1995a, ApJ, 444, 831

—. 1995b, ApJ, 444, 831

Höflich, P., Mueller, E., & Khokhlov, A. 1991, A&A, 248, L7

Howell, D. A., Sullivan, M., Nugent, P. E., et al. 2006, Nature, 443, 308

Hoyle, F. & Fowler, W. A. 1960, ApJ, 132, 565

Iben, Jr., I. & Tutukov, A. V. 1984, ApJS, 54, 335

Jeffery, D. J. & Branch, D. 1990, in Supernovae, Jerusalem Winter School for Theoretical Physics, ed. J. C. Wheeler, T. Piran, & S. Weinberg, 149–+

Jha, S., Garnavich, P. M., Kirshner, R. P., et al. 1999, ApJS, 125, 73

Kahabka, P. & van den Heuvel, E. P. J. 1997, ARA&A, 35, 69

Kasen, D. & Plewa, T. 2006, ArXiv Astrophysics e-prints

Khokhlov, A., Mueller, E., & Höflich, P. 1993, A&A, 270, 223

Khokhlov, A. M. 1991, A&A, 245, 114

Kirshner, R. P., Jeffery, D. J., Leibundgut, B., et al. 1993, ApJ, 415, 589

Knop, R. A., Aldering, G., Amanullah, R., et al. 2003, ApJ, 598, 102

Krisciunas, K., Phillips, M. M., Suntzeff, N. B., et al. 2004, AJ, 127, 1664

Krisciunas, K., Suntzeff, N. B., Candia, P., et al. 2003, AJ, 125, 166

Landsman, W. B. 1989, BAAS, 21, 784

Leibundgut, B., Kirshner, R. P., Filippenko, A. V., et al. 1991, ApJ, 371, L23

Lentz, E. J., Baron, E., Branch, D., & Hauschildt, P. H. 2001, ApJ, 547, 402

Leonard, D. C., Filippenko, A. V., Gates, E. L., et al. 2002, PASP, 114, 35

Li, W., Filippenko, A. V., Gates, E., et al. 2001a, PASP, 113, 1178

Li, W., Filippenko, A. V., Treffers, R. R., et al. 2001b, ApJ, 546, 734

Livne, E., Asida, S. M., & Höflich, P. 2005, ApJ, 632, 443

Lü, G., Yungelson, L., & Han, Z. 2006, MNRAS, 372, 1389

Marion, G. H., Höflich, P., Vacca, W. D., & Wheeler, J. C. 2003, ApJ, 591, 316

Marion, G. H., Höflich, P., Wheeler, J. C., et al. 2006, ApJ, 645, 1392

Massey, P. & Gronwall, C. 1990, ApJ, 358, 344

Massey, P., Strobel, K., Barnes, J. V., & Anderson, E. 1988, ApJ, 328, 315

Maxted, P. F. L., Marsh, T. R., & North, R. C. 2000, MNRAS, 317, L41

Mueller, E. & Höflich, P. 1994, A&A, 281, 51

Nomoto, K. 1982, ApJ, 253, 798

Nomoto, K. & Kondo, Y. 1991, ApJ, 367, L19

Nomoto, K., Thielemann, F.-K., & Yokoi, K. 1984, ApJ, 286, 644

Nomoto, K., Uenishi, T., Kobayashi, C., et al. 2003, in From Twilight to Highlight: The Physics of Supernovae, ed. W. Hillebrandt & B. Leibundgut, 115–+

Paczynski, B. 1985, in ASSL Vol. 113: Cataclysmic Variables and Low-Mass X-ray Binaries, ed. D. Q. Lamb & J. Patterson, 1–12

Patat, F., Benetti, S., Cappellaro, E., et al. 1996, MNRAS, 278, 111

Perlmutter, S., Deustua, S., Gabi, S., et al. 1997, in NATO ASIC Proc. 486: Thermonuclear Supernovae, ed. P. Ruiz-Lapuente, R. Canal, & J. Isern, 749–+

Phillips, M. M. 1993, ApJ, 413, L105

Phillips, M. M., Lira, P., Suntzeff, N. B., et al. 1999, AJ, 118, 1766

Piersanti, L., Gagliardi, S., Iben, I. J., & Tornambé, A. 2003, ApJ, 598, 1229

Plewa, T., Calder, A. C., & Lamb, D. Q. 2004, ApJ, 612, L37

Quimby, R., Höflich, P., Kannappan, S. J., et al. 2006, ApJ, 636, 400

Rappaport, S., Chiang, E., Kallman, T., & Malina, R. 1994, ApJ, 431, 237

Röpke, F. K., Niemeyer, J. C., & Hillebrandt, W. 2003, ApJ, 588, 952

Schlegel, D. J., Finkbeiner, D. P., & Davis, M. 1998, ApJ, 500, 525

Stetson, P. B. 1987, PASP, 99, 191

Stritzinger, M., Hamuy, M., Suntzeff, N. B., et al. 2002, AJ, 124, 2100

Struble, M. F. & Rood, H. J. 1999, ApJS, 125, 35

Umeda, H., Nomoto, K., Kobayashi, C., Hachisu, I., & Kato, M. 1999, ApJ, 522, L43

van den Heuvel, E. P. J., Bhattacharya, D., Nomoto, K., & Rappaport, S. A. 1992, A&A, 262, 97

Whelan, J. & Iben, I. J. 1973, ApJ, 186, 1007

Woosley, S. E. & Weaver, T. A. 1994, ApJ, 423, 371

Yamaoka, H., Nomoto, K., Shigeyama, T., & Thielemann, F.-K. 1992, ApJ, 393, L55

Table 1. Observing Log for HET Spectra of SN 2005hj

Date (UT)	JD-2400000.5	Phase (day)	Exp. (s)	Filter	Slit (″)
Oct 26.30	53669.30	-6	2x600	GG385	2.0
Oct 27.20	53670.20	-5	4x600	OG590	1.5
Oct 27.28	53670.28	-5	2x600	GG385	1.5
Nov 1.27	53675.27	0	2x600	GG385	1.5
Nov 1.29	53675.29	0	2x550	OG515	1.5
Nov 3.27	53677.27	2	2x480	GG385	1.5
Nov 4.26	53678.26	3	2x600	OG515	1.5
Nov 6.17	53680.17	5	2x600	GG385	1.5
Nov 6.18	53680.18	5	2x600	OG515	1.5
Nov 11.25	53685.25	10	3x600	OG515	1.5
Nov 19.22	53693.22	18	4x600	OG515	1.5
Nov 26.20	53700.20	25	2x600	OG515	1.5
Dec 5.18	53709.18	34	3x600	OG515	2.0

Note. — Phases are relative to the derived date of maximum light, 2005 Nov. 1.6, and rounded to the nearest day. Effective wavelength ranges for the GG385, OG515, and OG590 setups are 4100-8900 Å, 5100-9800 Å, and 5900-10,800 Å, respectively. All spectra from a given night were combined for the figures and analysis.

Table 2. Derived Quantities for the SN 2005hj Si II λ6355 Line

Phase (days)	Velocity (km s^{-1})	$\sigma_{\rm vel}$ (km s^{-1})	Depth[a]	FWHM (Å)
−6	10820	140	0.38	140
−5	10800	110	0.32	120
0	10640	90	0.52	110
2	10440	100	0.60	110
3	10640	90	0.57	110
5	10680	80	0.57	110
10	10530	100	0.60	100
18	10550	120	0.48	90
25	9850	90	0.25	60
34	...	...	...	...

Note. — Quantities measured from the FT smoothed data. The Si II λ6355 line is not clearly detected in the +34 day spectrum and thus no measurements are reported.

[a]Similar to Leonard et al. (2002), depth is defined as $(f_c - f_{\rm min})/f_c$ where $f_{\rm min}$ is the flux at the minimum of the smoothed line and f_c is the estimated continuum level at the corresponding wavelength.

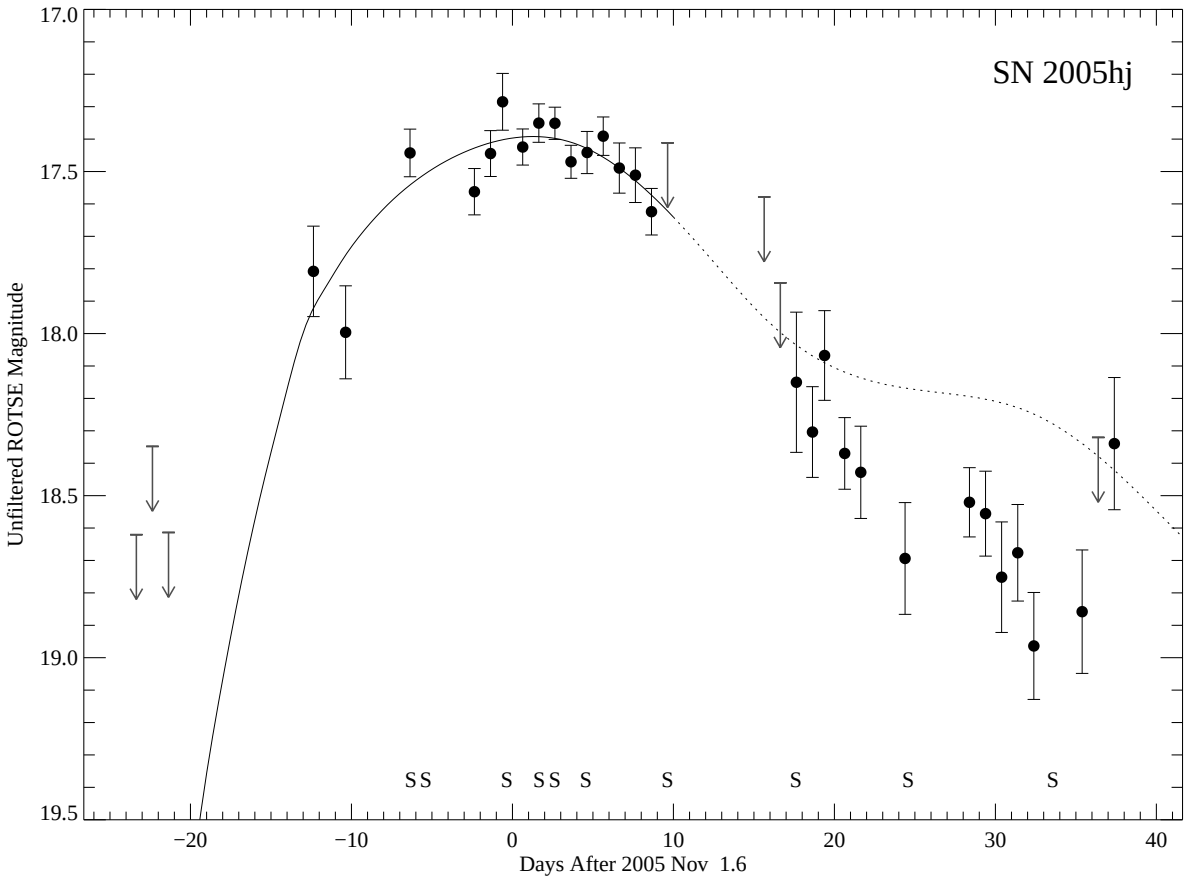

Fig. 1.— ROTSE-IIIb unfiltered light curve of SN 2005hj (filled circles). The best fit R-band template from Knop et al. (2003) is plotted as a solid line over the fitting range, and as a dotted line continuing on to later phases when the rapid decline of the flux below ∼5500 Å causes our unfiltered light curve to fade faster than the R-band decline rate. Arrows mark 5-σ upper limits of the subtractions determined from the noise level in annuli centered on the location of the SN. Epochs with HET spectra are marked with "S."

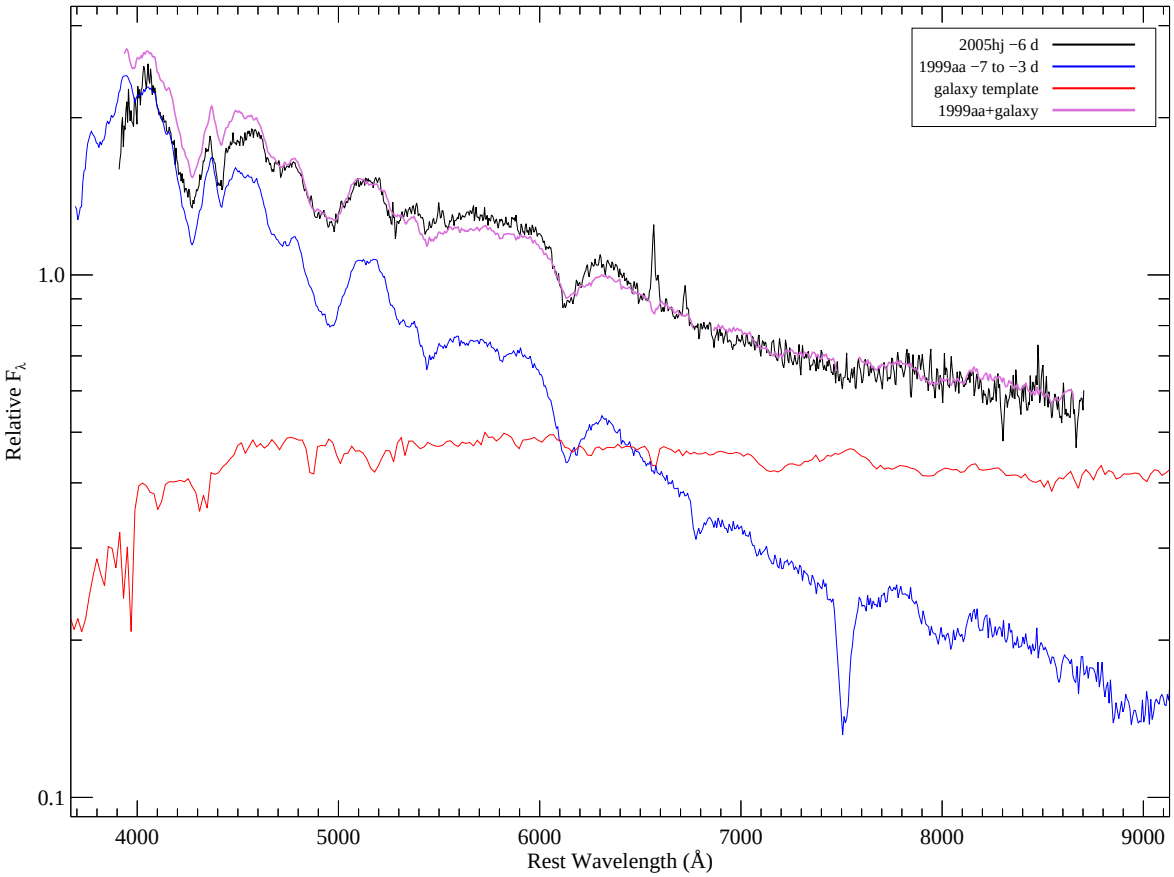

Fig. 2.— HET/LRS spectrum of SN 2005hj at −6 days (black line). The blue curve shows the relative contribution from a SN 1999aa-like supernova at the same phase from a linear interpolation of the −7 and −3 day spectra presented by Garavini et al. (2004), and the red line gives the estimated relative host galaxy light contamination. The relative scaling for the galaxy and SN components were determined through a least squares fit to the SN 2005hj spectrum. The purple line shows the fit (portions of the spectra effected by telluric lines were excluded from the fitting as shown by gaps in the fit curve).

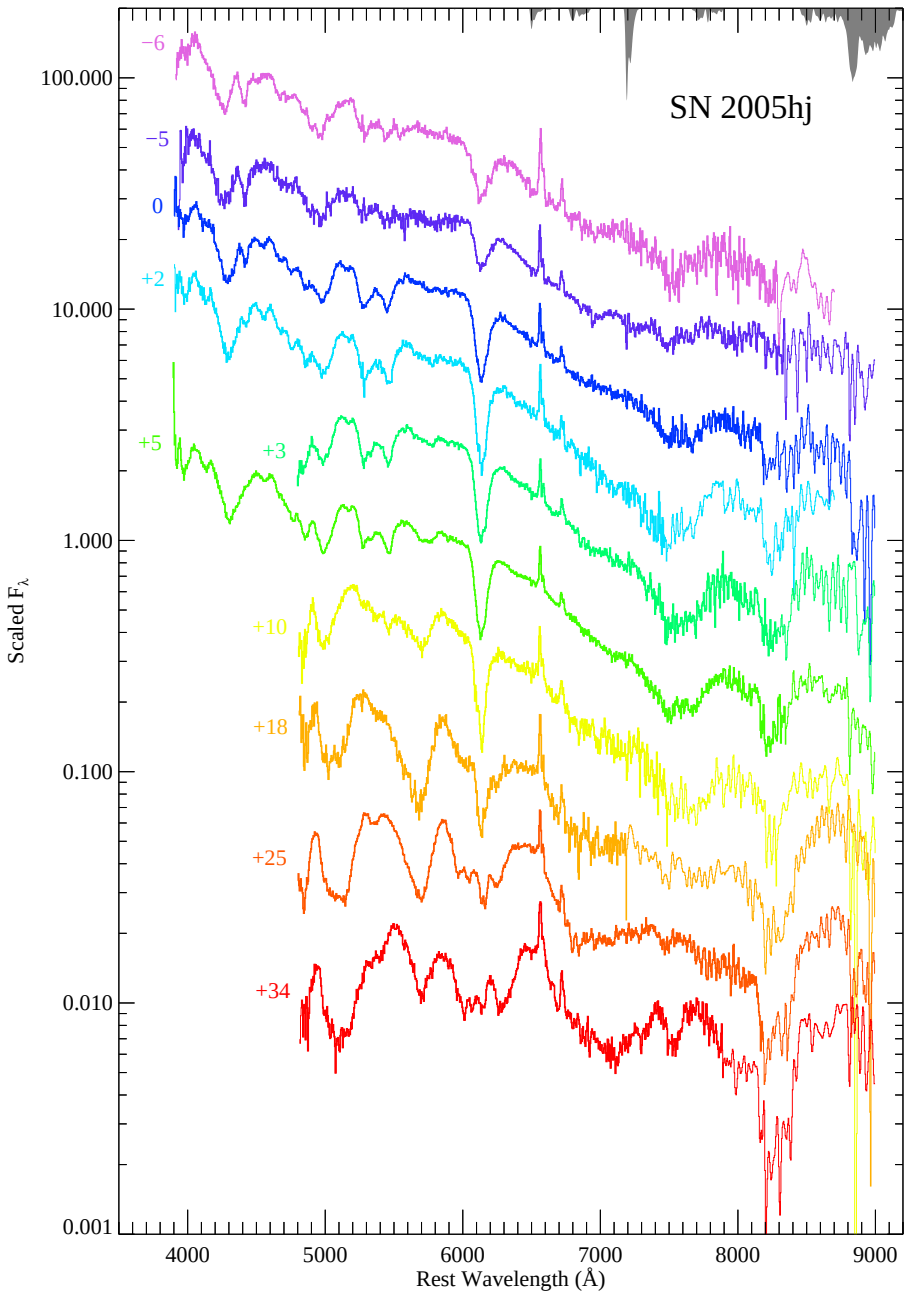

Fig. 3.— Spectral evolution of SN 2005hj recorded by the HET from −6 to +34 days after maximum light (2005 Nov. 1.6). The estimated galaxy contamination has been subtracted and the spectra have been shifted for clarity. For display purposes, portions of the spectra with low signal to noise have been smoothed (thin line segments). The typical telluric absorption spectrum is shown by the grey shading along the top of the figure.

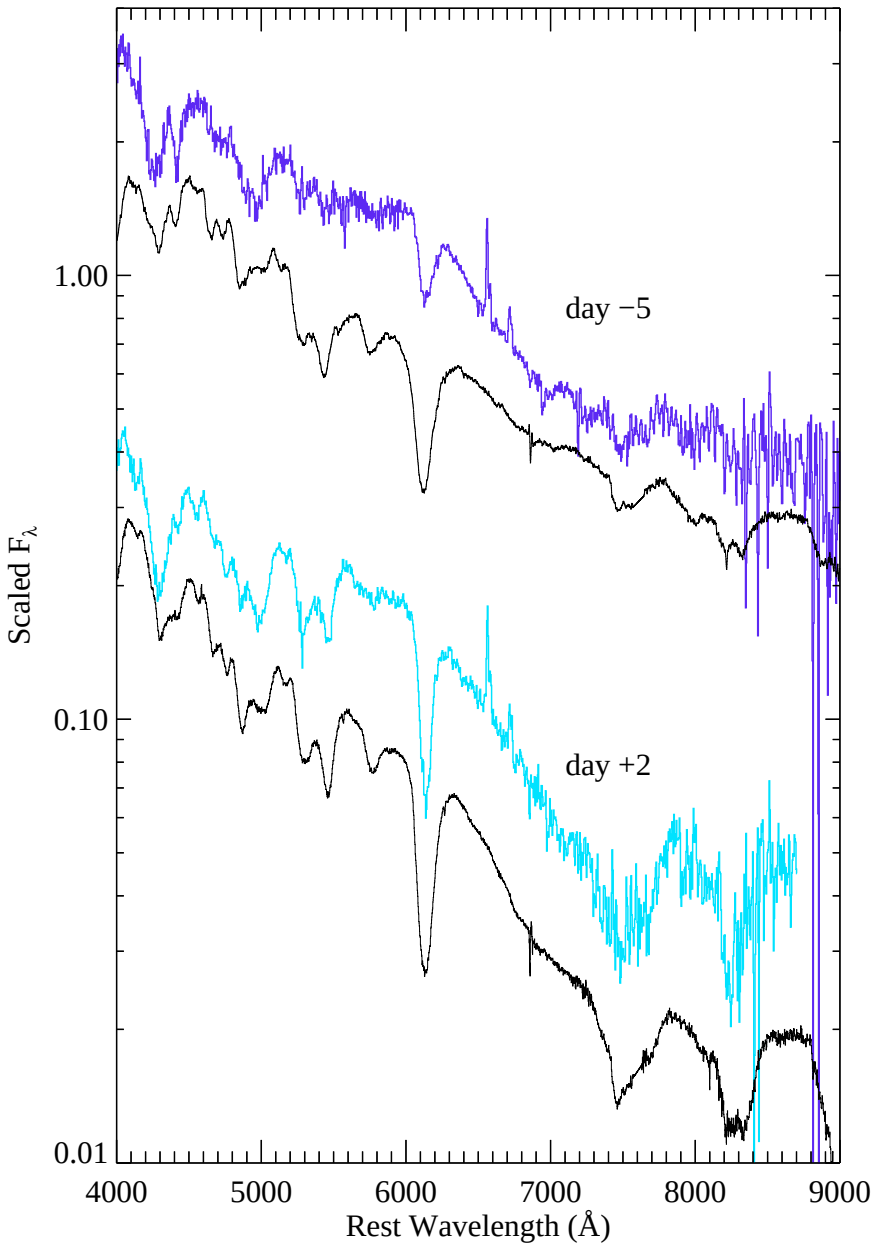

Fig. 4.— Comparison of the spectra of SN 2005hj (colored lines) and SN 1994D (black lines; Patat et al. 1996) at 5 days before and 2 days after maximum light. The spectra have been shifted for clarity. At both phases shown, the absorption component of the Si II λ6355 line is more narrow for SN 2005hj. The relative line depths for this feature are similar at +2 days, however, the Si II λ6355 absorption is much weaker for SN 2005hj in the −5 day spectrum. Despite these differences, the velocities inferred from the minima of the Si II λ6355 lines are consistent between SN 2005hj and SN 1994D to within 5%, the former being 560 km s^{-1} slower at −5 days and 150 km s^{-1} slower at +2 days.

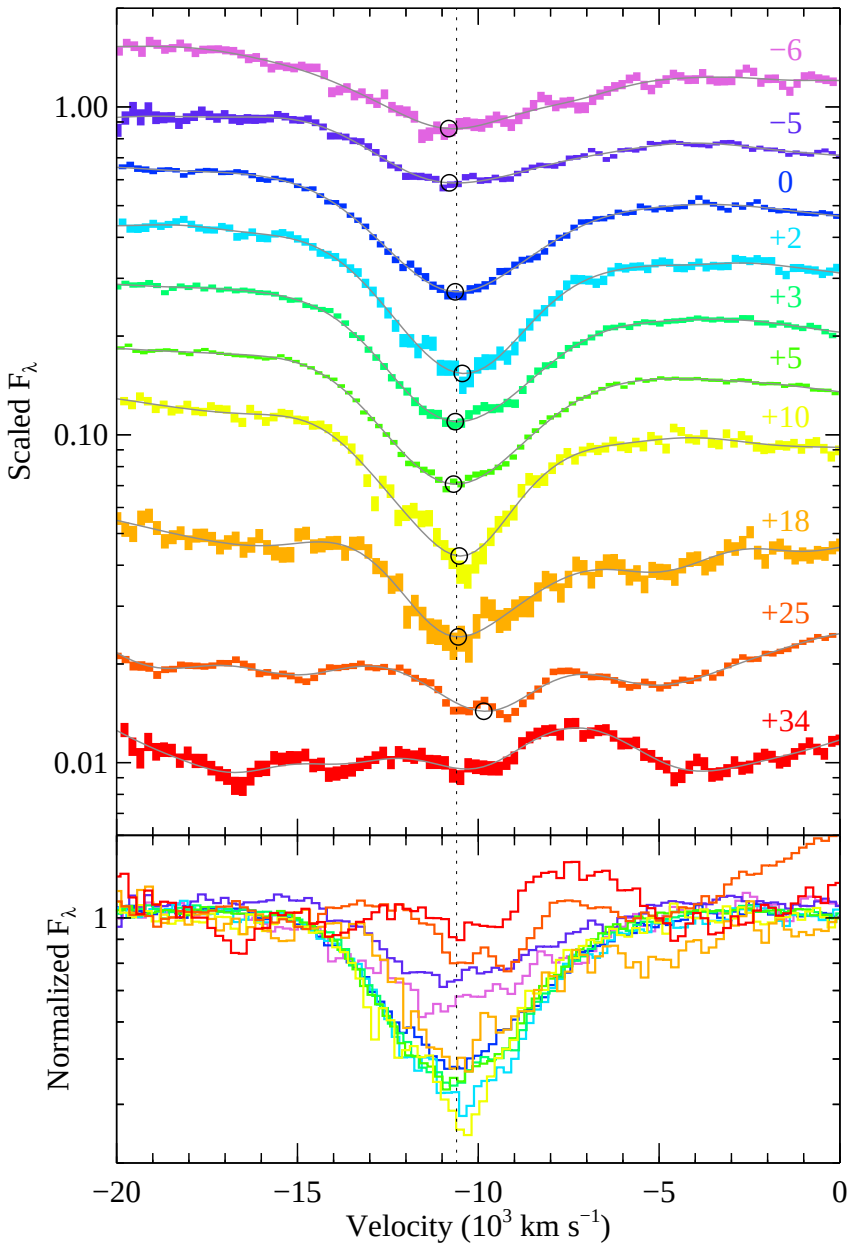

Fig. 5.— Evolution of the Si II λ6355 line. In the top plot, the spectra have been shifted by arbitrary factors for clarity with the youngest spectrum on the top and the oldest on the bottom, and they are colored as in figure 3. Each spectral bin is plotted as a rectangle with the height indicating the statistical 1-σ error interval. The effects of the FT smoothing are shown by the grey curves, and open circles mark the FT smoothed minima. The bottom plot shows the data normalized by the continua to emphasize the relative spectral evolution. The vertical dashed line marks the plateau velocity of 10,600 km s^{-1}.

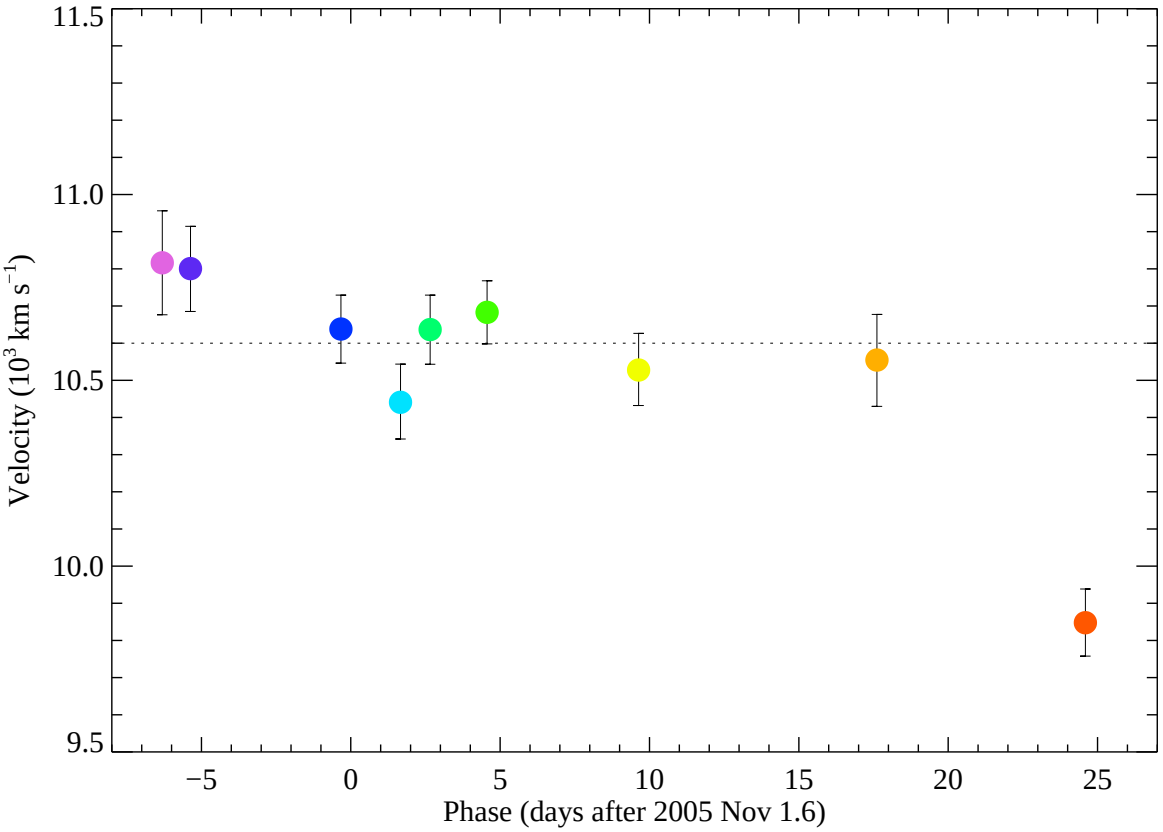

Fig. 6.— Velocity of the Si II λ6355 line minimum as determined from the FT smoothed minima. The error bars are the quadrature sum of the 1-σ confidence intervals found via Monte Carlo simulations and the 80 km s^{-1} scatter found in the H II region line centers among the different epochs.

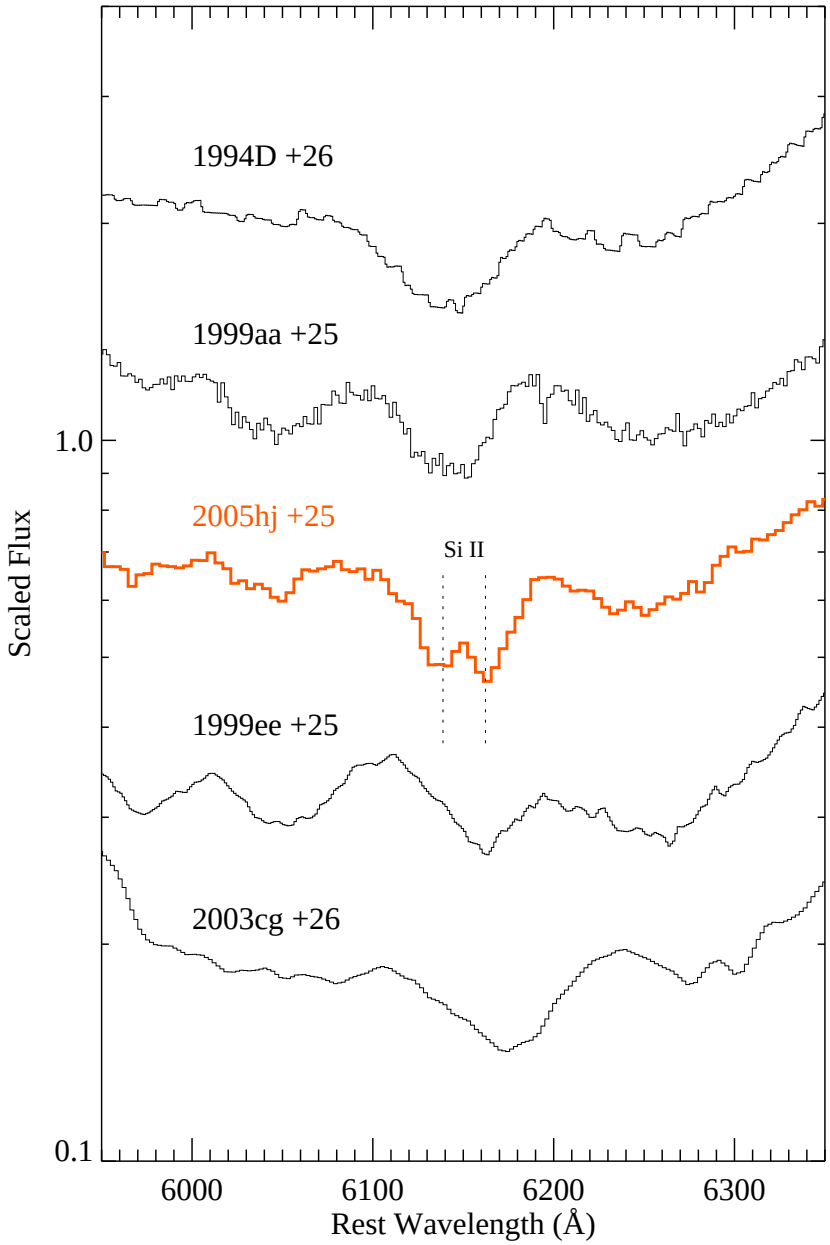

Fig. 7.— Spectra near the Si II λ6355 doublet for SN 2005hj and other SNe Ia around 25 days after maximum light (1994D; Patat et al. 1996; 1999aa; Garavini et al. 2004; 1999ee; Hamuy et al. 2002; 2003cg; Elias-Rosa et al. 2006). Vertical dotted lines mark the doublet components blue shifted by 10,000 km s^{-1}. The doublet is clearly resolved only in the case of SN 2005hj, while the flat bottom to the SN 1999aa profile may suggest similar behavior.

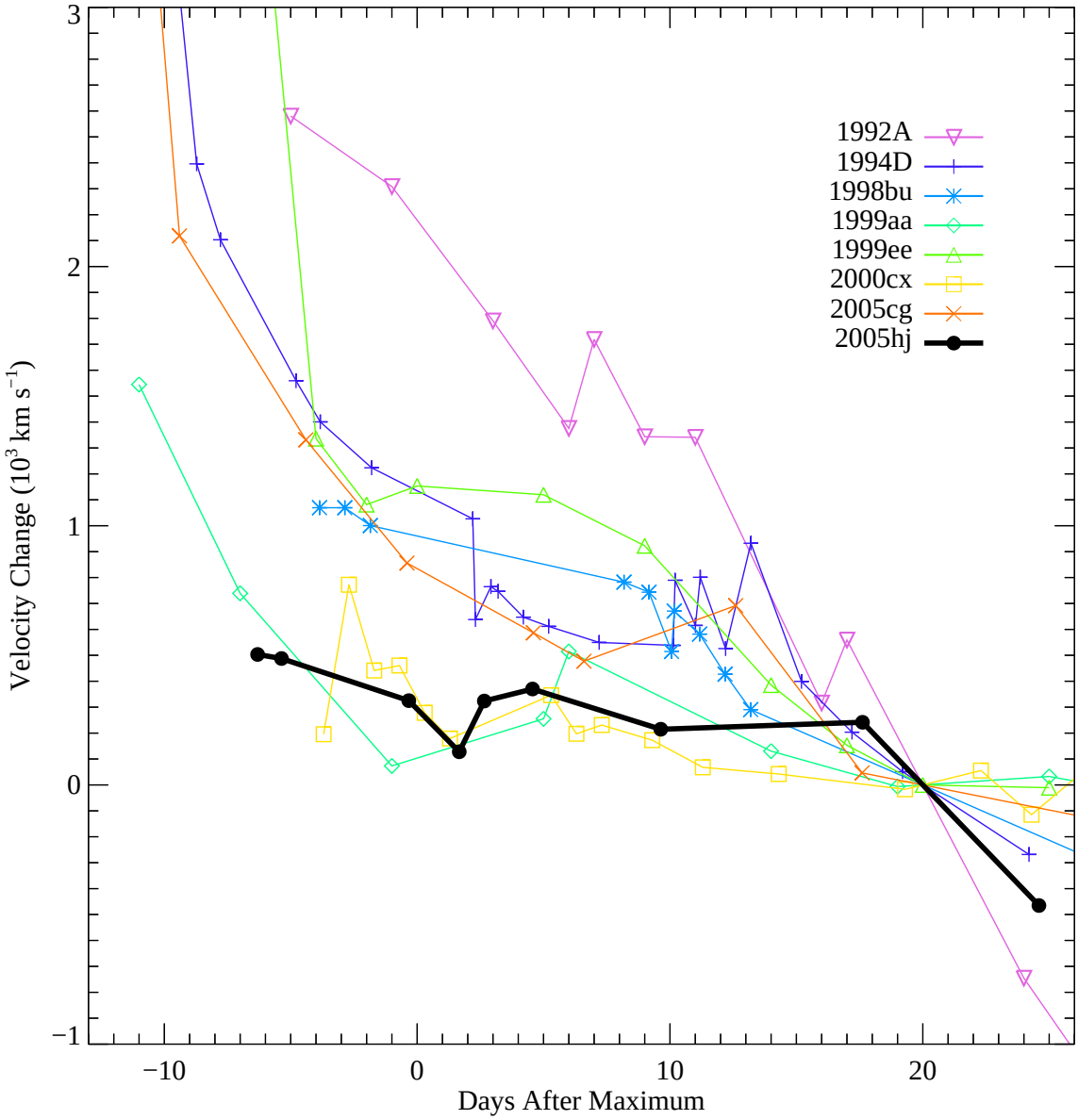

Fig. 8.— Velocity of the Si II λ6355 line minima for SN 2005hj and other well-observed SNe Ia (1992A; Kirshner et al. 1993; 1994D; Patat et al. 1996; 1998bu; Jha et al. 1999; 2000cx; Li et al. 2001a; 1999aa; Garavini et al. 2004; 1999ee; Hamuy et al. 2002; 2005cg; Quimby et al. 2006). All velocities were calculated from the FT smoothed minima using the same filter. The ordinate shows the change in velocity relative to the (interpolated) day +20 value. Lines connecting the data points are intended only to guide the eye. The sample was not drawn randomly from the parent population; instead it was tailored to show the range of behaviors present in well-observed in normal-bright events.

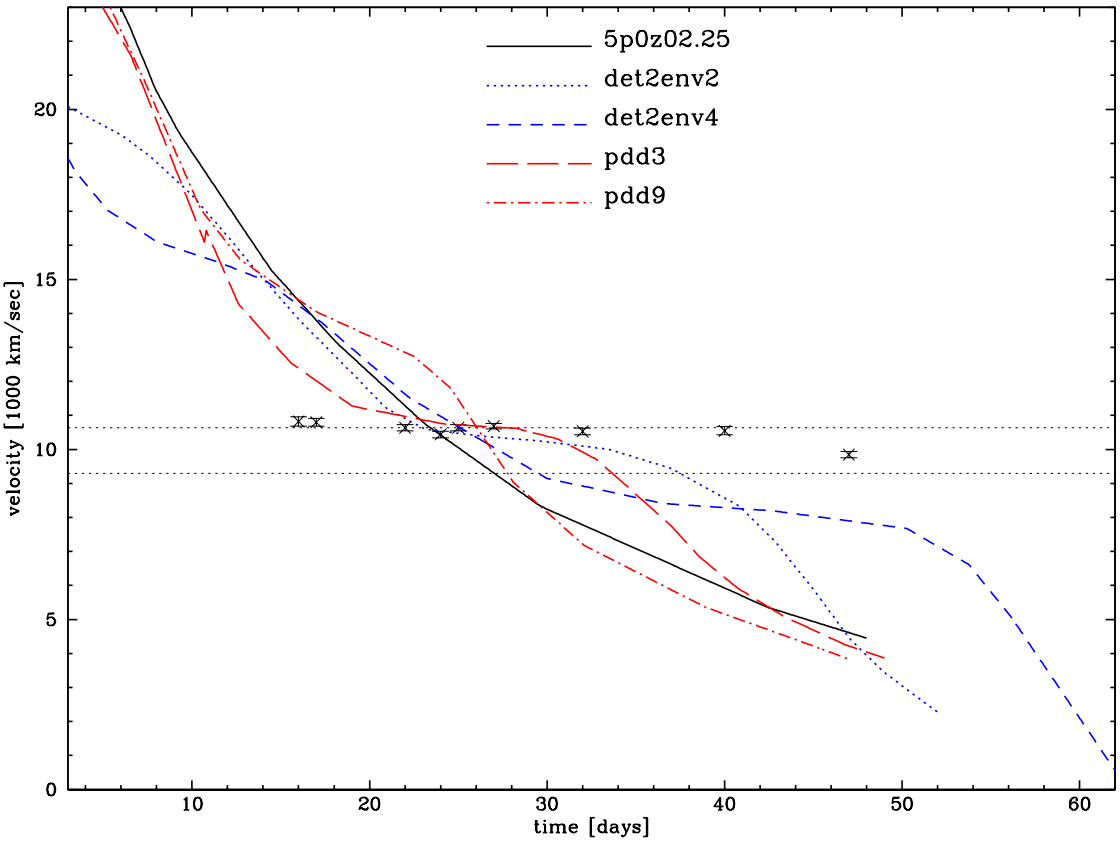

Fig. 9.— Photospheric velocity versus time since explosion for models of Branch-normal SNe Ia. The photosphere is defined by the radius of last scattering, and because Thomson scattering is the dominate source of continuum opacity, this position is largely wavelength independent. Shown are the classical delayed detonation model `5p0z02.25` (Höflich et al. 2002), the pulsating delayed detonation models `pdd3` and `pdd9` (Khokhlov et al. 1993; Höflich et al. 1995b), and the tamped detonation models `det2en2/4` (Höflich & Khokhlov 1996). The X's mark the velocities of SN 2005hj as measured from the minima of the Si II λ6355 line assuming a 22 day rise to peak. The dotted horizontal lines mark the region with $> 1\%$ Si abundance in model `pdd3`. As discussed in the text, the Si II λ6355 line minimum is an imperfect indicator of the photospheric velocities, and a systematic offset can develop at later times once the photosphere has receded below the Si rich layers. This may explain the discrepancy between the model predictions and the last two observations, which show weakening Si and strengthening Fe lines. The low velocities observed at early times for SN 2005hj may indicate that rather little outward mixing took place.

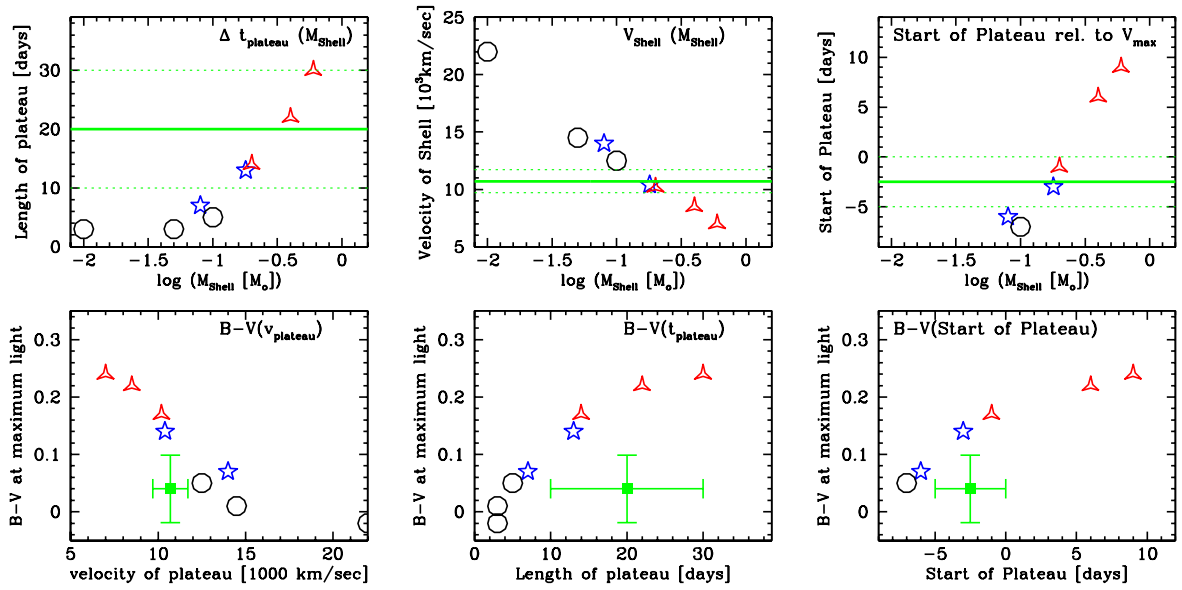

Fig. 10.— Properties of Branch-normal SNe Ia models with interacting shells of mass M_{Shell} including delayed detonations (`5p0z22.25` with $M_{Shell} = 0.01, 0.05$ and $0.1 M_\odot$, open circles Gerardy et al. 2004), pulsating delayed detonation models (open stars; `pdd3`; Khokhlov et al. 1993; Höflich & Khokhlov 1996; `pdd9`; Höflich et al. 1995b) and merger models (open triangles; `det2env2/4/6`; Khokhlov et al. 1993; Höflich & Khokhlov 1996). In the upper plots, we give as a function of M_{Shell} the duration of the velocity plateau $\Delta t_{plateau}$, its velocity $v_{plateau}$ defined by $\delta v \leq 500$ km s^{-1} (see text), and its starting point t_0 relative to maximum light. In the lower plots we give observational relations, namely $B-V$ at maximum light as a function of $v_{plateau}$, $\Delta t_{plateau}$ and t_0. Note that $B-V$ is uncertain by about 0.05 to 0.1^m. In addition, we give the observations of SN 2005hj (filled squares) including error bars.